Coupling long-term GNSS monitoring and numerical modelling of lateral spreading for hazard assessment purposes

Matteo Mantovani[a], Giulia Bossi[a]*, Alan P. Dykes[b], Alessandro Pasuto[a], Mauro Soldati[c], Stefano Devoto[d]

[a]*National Research Council, Research Institute for Geo-Hydrological Protection (IRPI), corso Stati Uniti 4, 35127 Padova, Italy*

[b]*Centre for Engineering, Environment and Society Research, School of Engineering and Environment, Kingston University, Penrhyn Road, Kingston upon Thames KT1 2EE, UK*

[c]*Department of Chemical and Geological Sciences, University of Modena and Reggio Emilia, via Campi 103, 41125 Modena, Italy*

[d]*Department of Mathematics and Geosciences, University of Trieste, via A. Weiss 2, 34127 Trieste, Italy*

**Corresponding author: giulia.bossi@irpi.cnr.it, corso Stati Uniti 4, 35127 Padova, Italy*

Abstract

Lateral spreading is a complex geomorphological process occurring through the interplay of different factors. Due to their low rates of displacement, lateral spreads in rock are much less investigated than other landslide types even though sometimes they can evolve into faster and more hazardous movements such as topples. The lack of long-term monitoring data means that the deformation mechanisms of these landslides remain uncertain. Along the northwestern coast of the island of Malta (central Mediterranean Sea), the presence of a thick layer of clay underlying a brittle cap rock made of limestone has led to extensive rock spreading and associated block sliding. Two sites affected by such processes were monitored by GNSS (Global Navigation Satellite Systems) from 2005 to 2019. A network consisting of 17 benchmarks were surveyed twice per year, providing a 14-year displacement history. Coupling this exceptionally long monitoring dataset with Limit Equilibrium and Finite Difference slope stability modelling, the failure mechanisms of the landslides have been investigated to identify predisposing and driving instability factors. This research provides new knowledge on the kinematic behavior of extremely slow landslides and insights into landslide hazard assessments in areas extensively affected by lateral (rock) spreading.

Keywords: lateral spreading, GNNS monitoring, numerical modelling, hazard assessment, Malta

1. Introduction

Large sectors of the coasts in the Mediterranean Sea are affected by landslides (Kirschbaum et al., 2010) that often pose a threat for tourist facilities and sometimes heritage sites (Fiorillo, 2003; Della Seta et al., 2013; Miccadei et al., 2019; Rizzo et al., 2020). Deep-seated Gravitational Slope

Deformations (DGSDs) of the lateral spreading type - consisting of rock spreads often evolving into block slides - are common along the coasts of Spain (Mateos et al., 2018; Tomas et al., 2018), Italy (Carobene and Cevasco, 2011; Agnesi et al., 2015; Ietto et al., 2015), Greece (Ilia et al., 2015), Malta (Soldati et al., 2019, Devoto et al., 2021) and Morocco (Bounab et al., 2021). Lateral spreading mainly gives rise to planar movements resulting in the cracking of a resistant but brittle rock mass capping a layer made of softer and more deformable materials such as clays or marls (Pasuto and Soldati, 2013). Lateral spreading is characterized by extremely slow rates of movements. According to Cruden and Varnes (1996) landslide movement scale, the terms "extremely slow" and "very slow" refer to mass movements with a rate range from 0 to 16 mm per year and from 16 mm per year to 1.6 m per year, respectively. Block slides are downslope movements along a slip surface that can involve resistant materials in conjunction with clayey lithologies. The slip surface is markedly non-circular, characterized by a vertical main scarp in the crown area, as a result of the fracturing and subsidence of the rock masses. The inclination of the slip surface can change abruptly and become flat resulting in mainly horizontal displacements at the toe.

The hazard associated with slow-moving landslides is generally underestimated compared with other types of mass movements (Mansour et al., 2011), despite the fact that some types can evolve into faster and catastrophic events due to external triggering factors (seismic or meteorological) or when a modification of their geometry reaches a state of marked disequilibrium. As reported by Lacroix et al. (2020), slow-moving landslides move downslope for months to decades or centuries with rates that can vary from millimeters to several tens of millimetres per years, developing different types of landforms such as gravity-induced joints, graben, trenches, rock pillars, bulges and hummocky terrains (Pánek and Klimeš, 2016; Mariani and Zerboni, 2020).

To perform accurate analyses and classifications of such mass movements, detailed mapping of landslide areas and associated landforms as well as assessments of the surface displacements in terms of magnitude and patterns is necessary (Angeli et al., 2000; Arosio et al., 2019). A long-term monitoring programme hence represents a fundamental requirement to improve our understanding of the failure mechanism and kinematics of extremely slow landslides, and provides the basis for disaster prevention and early-warning management studies (Petley et al., 2005). The use of Remote Sensing (RS) techniques in landslide mapping and monitoring, such as LiDAR (Light Detection And Ranging) surveys, Synthetic Aperture Radar Interferometry (InSAR) and Uncrewed Aerial Vehicle - Digital Photogrammetry (UAV-DP), has vastly expanded over the last two decades, thanks to the increasing number of space missions, technological progress in sensor development and the advances of new algorithms (Casagli et al., 2017; Toth and Jóźków, 2016). Scaioni et al. (2014) provided a RS review mainly focused on InSAR and LiDAR techniques in landslide investigations. Nowadays space-borne DInSAR (i.e. Differential InSAR) is one of the most reliable techniques to measure ground displacements over large areas with extremely high accuracy. Moreover, since the development of the approaches commonly referred to as Advanced DInSAR (A-DInSAR) or Time Series Radar Interferometry (TS-InSAR) some 20 years ago, it is possible to reconstruct historical analysis of the displacements and perform long-term measurements. Nevertheless, the practical applicability of A-DInSAR analysis to study landslides is still problematic since it is inherently related to the size, the aspect and the inclination of the slope, to land cover and to the velocity and mechanisms of displacement (Colesanti and Wasoswki, 2006, Mantovani et al., 2019). Furthermore, there are no guarantees that informative points (i.e. persistent scatterers, coherent points) can be detected in the area of interest prior several steps of data processing that can be demanding in computational terms and costs. To conclude, the observables

are ranges measured along the sensor-target line of sight and it is not possible to derive the real direction of the displacements unless *a priori* assumptions are made.

Topographic monitoring systems such as GNSS surveys and Automated Total Station (ATS) measurements have been more commonly used in landslides monitoring (Gili et al., 2000; Malet et al., 2002; Coe et al., 2003; Corsini et al., 2005; Peyret et al., 2008; Wang, 2012; Palis et al., 2017). There are many reasons for this including the ability to choose the spatial and temporal sampling of the measurements, the minimum expertise and the reduced computational effort required to calculate the displacement vectors and interpret the results. Nevertheless, it is quite unusual in scientific literature to find lateral spreads that have been monitored for more than few years (Table 1).

Table 1. Scientific papers dealing with the monitoring of lateral spreading.

Reference	Location	Monitoring Technique	Period of investigation
Agnesi et al., (2015)	Scopello (Italy)	GNSS	2000-2005
Ietto et al., (2015)	Tropea (Italy)	A-DInSAR	1993-2000
Mateos et al., (2018)	Bàlitx (Spain)	A-DInSAR	2007-2010
Tomas et al., (2018)	Alicante (Spain)	ATS	2011-2015

This is mainly related to the great effort required to maintain a monitoring network. The displacements occurring over the landslide often damage the GNSS benchmarks or make access to them unsafe. Several times measuring points are simply lost as the result of acts of vandalism. Finally, GNSS monitoring is preferred to investigate rapid landslides, since it provides a quicker response in terms of hazard assessment (Tagliavini et al., 2007).

The aim of this study was to determine whether the stability and failure conditions of rock spreads on Malta can be established using standard modelling approaches (Limit Equilibrium and Finite Difference), given that a means of validating the modelling results is provided by displacement data from a 14-year GNSS monitoring campaign. Two rock spreads on the northwestern coast of Malta were the focus of this work. Although slightly different in the details of their local characteristics and contexts, the two sites are only 4 km apart and contain the same geological units. As such, they can be considered representative of the many similar landslides around the entire northwestern and northern coastlines of Malta and elsewhere. This study builds on previous work to characterise the geological and geomorphological hazards of this Maltese coastline in terms of its extensive suite of mass movement (Mantovani et al., 2013, 2016; Piacentini et al., 2015). In doing so, it presents a novel and potentially highly significant development in engineering geology in the form of a new approach for the analysis and hazard assessment of lateral spreads more widely, especially as it is now be possible to obtain and integrate displacement measurements from different satellite platforms over periods of more than 20 years (e.g. Di Martire et al., 2016) to support modelling analyses of individual landslides.

2. Study area

The Maltese archipelago, formed by three main islands –Malta, Gozo and Comino– and a group of uninhabited islets, is the result of complex geodynamical processes that shaped the Central Mediterranean 10 million years ago and are still active today (Figure 1). The stratigraphy of the islands consists of five geological formations: Lower Coralline Limestone (LCL), Globigerina Limestone (GL), Blue Clay (BC), Greensand (GS) and Upper Coralline Limestone (UCL). The

thickness of the GS, consisting of glauconitic sand bed, is usually less than 0.5 m or absent on Malta but is much thicker on Gozo (Scerri, 2019). The UCL is exposed in the northwestern part of Malta and is subdivided into four members. The Mtarfa Member (MM) is the most recognizable and the weakest of the members, being characterized by light yellow cream or white limestones and marls.

This simple stratigraphic sequence of sedimentary rocks with differing lithostratigraphic properties has been intensely faulted, tilted and weathered giving rise to a large variety of landscapes (Galea, 2019). Some of the most spectacular landforms can be found in the northwestern sector of Malta, where the BC is exposed at sea level and capped by low-altitude UCL plateaus. Along this stretch of the coast, 'rdum' (scree slopes in Maltese) morphology is common, as a consequence of the breaking off of the UCL caprock and their resulting toppling and sliding down over the gentle slopes made of BC, towards the sea or until reaching the shore platforms made of GL (Gauci and Scerri, 2019).

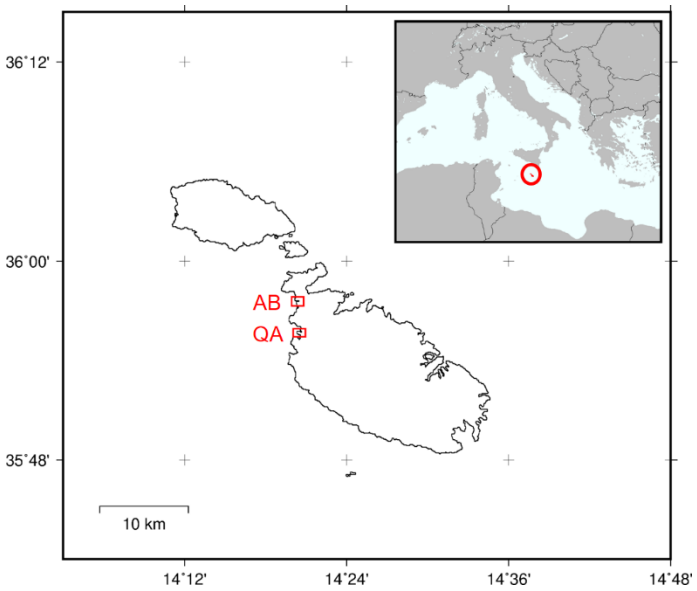

Figure 1. The Maltese islands with the location of the two study sites: Il-Qarraba (QA) and Anchor Bay (AB).

2.1 Il-Qarraba

The head-shaped peninsula of Il-Qarraba (35°55'38.5"N 14°20'29.0"E) is located between Gnejna Bay and Ghajn Tuffieha Bay. It is formed by an Upper Coralline Limestone caprock, 7 to 23 m thick, overlying the Blue Clay to a height of about 40 m a.s.l. (Figure 2). The basal portion of the plateau is made up of the Mtarfa Member and gently dips towards outer Ghajn Tuffieha Bay.

Lateral spreading affects the plateau, as observed by a complex network of joints mapped by Devoto et al. (2020) using UAV-Digital Photogrammetry. Most of these gravity-induced open joints are vertical, affecting the entire thickness of the Upper Coralline Limestone rock cap and with lengths varying from 7 m to 100 m. The lateral spreads evolve into large block slides as witnessed by tens of blocks scattered over the Blue Clay slopes. Most of these Upper Coralline Limestone blocks preserve their original shape and are partially sunk in the substratum, others are tilted as a result of a sliding or a toppling. The compression created by the block sliding on the clayey terrains, has generated bulges, depressions and hummocks on the slopes. This morphology is more pronounced in the northern and western sectors of the peninsula. Along with the slow-moving mass

movements several other “collateral” landslides also occur; small earth flow/slides along the steep and bare clayey slopes forming the thin isthmus that connects Il-Qarraba to the mainland and rock falls mainly affecting the Mtarfa Member at the margins of the steep cliffs of the cap rock (Devoto et al., 2013b).

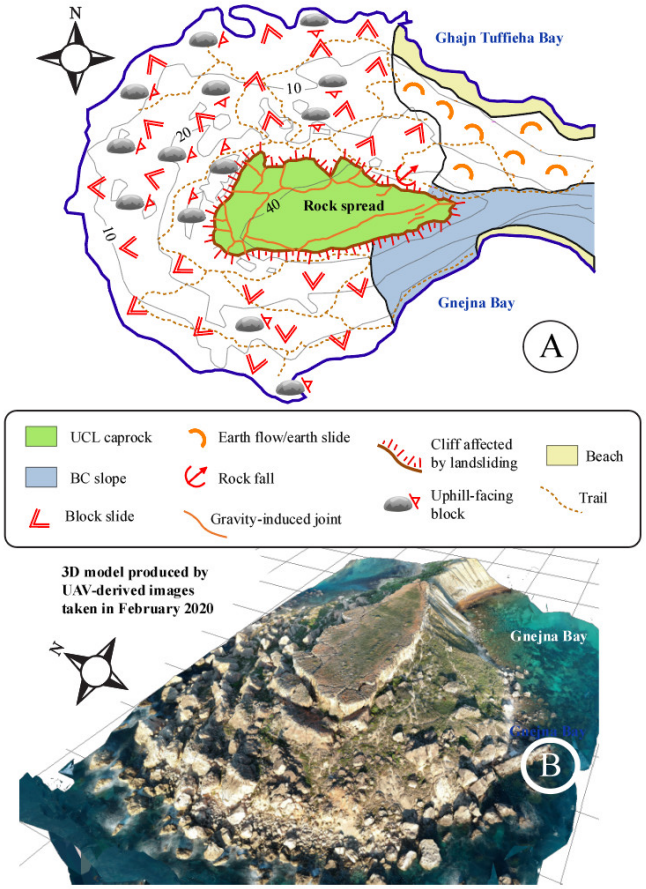

Figure 2. A) Geomorphological sketch of Il-Qarraba. **B)** 3D reconstruction of Il-Qarraba from UAV-DP.

2.2 Anchor Bay

Anchor Bay (35°57'39.0"N 14°20'23.2"E) is a structurally controlled cove less than 4 km north of Il-Qarraba (Figure 3). The Upper Coralline Limestone promontory that borders the northern part of the inlet is affected by lateral spreading which has evolved into spectacular block slides below the western half of the cliffs (Devoto et al., 2012). Above the eastern part of the cliffs, the plateau is affected by rock spreading that produces persistent vertical and subvertical discontinuities (Devoto et al., 2020), displacing the limestone cap by up to 2 m. Below the edge of the plateau the cliff is steep and about 20 m high, exposing the Mtarfa Member for about half of its length. This cliff, the headscarp of a distinct landslide system, separates the plateau from a remarkably displaced and cracked unit oriented approximately parallel to the coast (Soldati et al., 2019). The tilted and displaced limestone blocks scattered along the Blue Clay slopes on the north side of the bay have produced a rugged morphology that is often thought to be spectacularly scenic. For this reason, the site was used as the

location for a movie sets and has subsequently been transformed through the years into an amusement park which attracts a high number of visitors each year. The presence of an E-W oriented fault running across the inlet resulted in a completely different morphology of the opposite side of the bay. The southern margin of Anchor Bay is in fact down-faulted, exposing the Upper Coralline Limestone formation at sea level to give a plunging cliff of about 25 m in height.

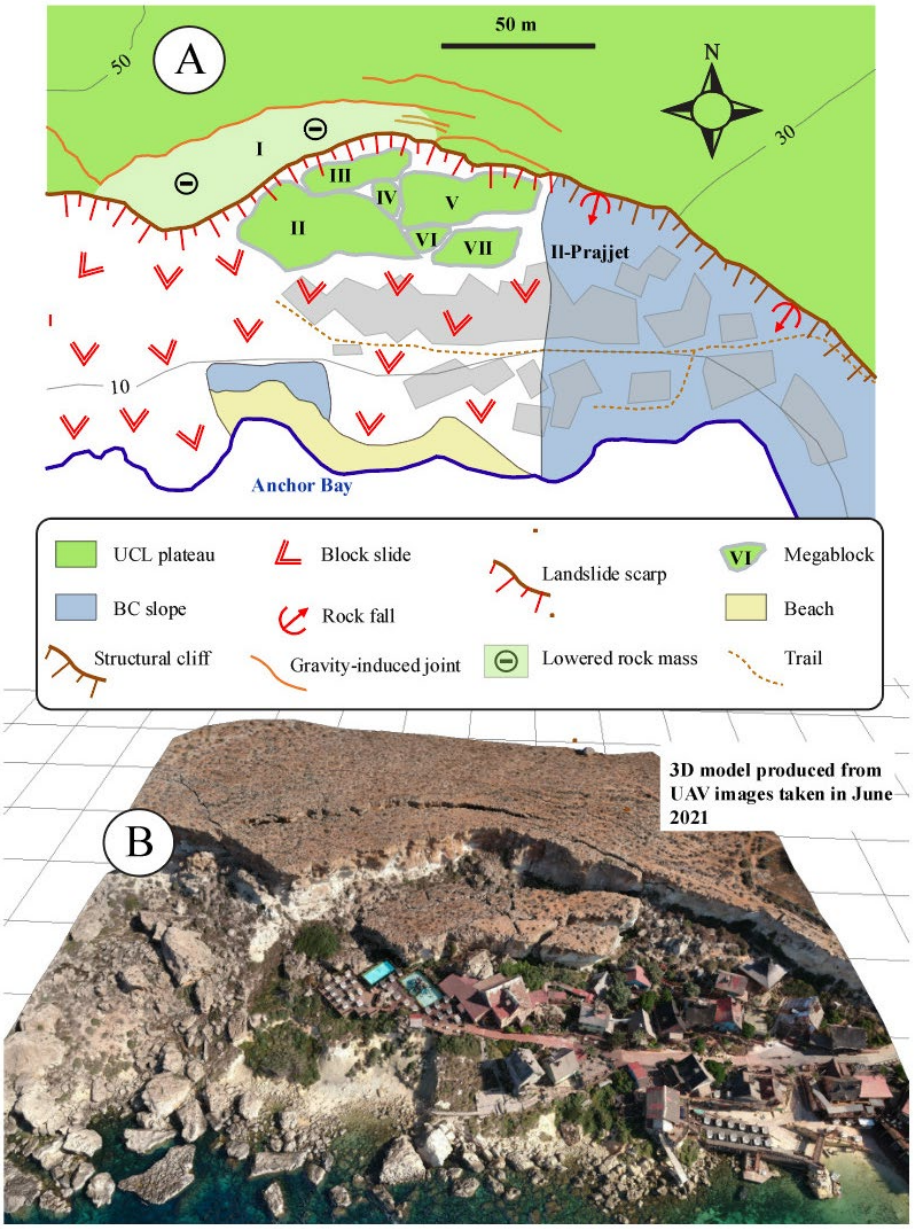

Figure 3. A) Geomorphological sketch of Anchor Bay. **B)** 3D reconstruction of Anchor Bay from UAV-DP.

3. GNSS monitoring network

The Global Navigation Satellite System (GNSS) is an all-weather, space-based navigation

system, that uses electromagnetic signals broadcast by a constellation of artificial satellites to determine the position and instantaneous velocity of a receiver in a common reference system (Hofmann-Wellenhof et al., 2001). An exhaustive description of the theoretical principles and its application to landslide monitoring can be found in Gili et al. (2000). There are several mathematical models that make use of the GNSS constellation for positioning, which are distinguished according to the number of the receivers employed during a survey, the tracked components or the signal, the time of acquisition at each point and the processing methodology. The static relative positioning is the more accurate of these models and is the one used in this study.

The GNSS monitoring network was installed at the two test sites at the end of the summer 2005, since then 27 surveys were performed at Il-Qarraba and 25 at Anchor Bay, twice per year until spring 2019. The survey benchmarks comprised steel rods drilled into the Upper Coralline Limestone to assure a good coupling with the ground. Their heads, which stand about 0.1 m above the ground, were shaped to join perfectly with the receiving antenna, allowing the removal of positioning errors. The network originally consisted of 9 measurement benchmarks at Il-Qarraba and 8 at Anchor Bay, but during the years several were damaged, others removed and a few more re-installed in other locations (Figure 4). Two reference stations, one for each test site, were installed nearby in areas considered to be stable from a geological and geomorphological viewpoint. At the time of the last survey, 6 survey benchmarks were still usable at Il-Qarraba and 7 at Anchor Bay.

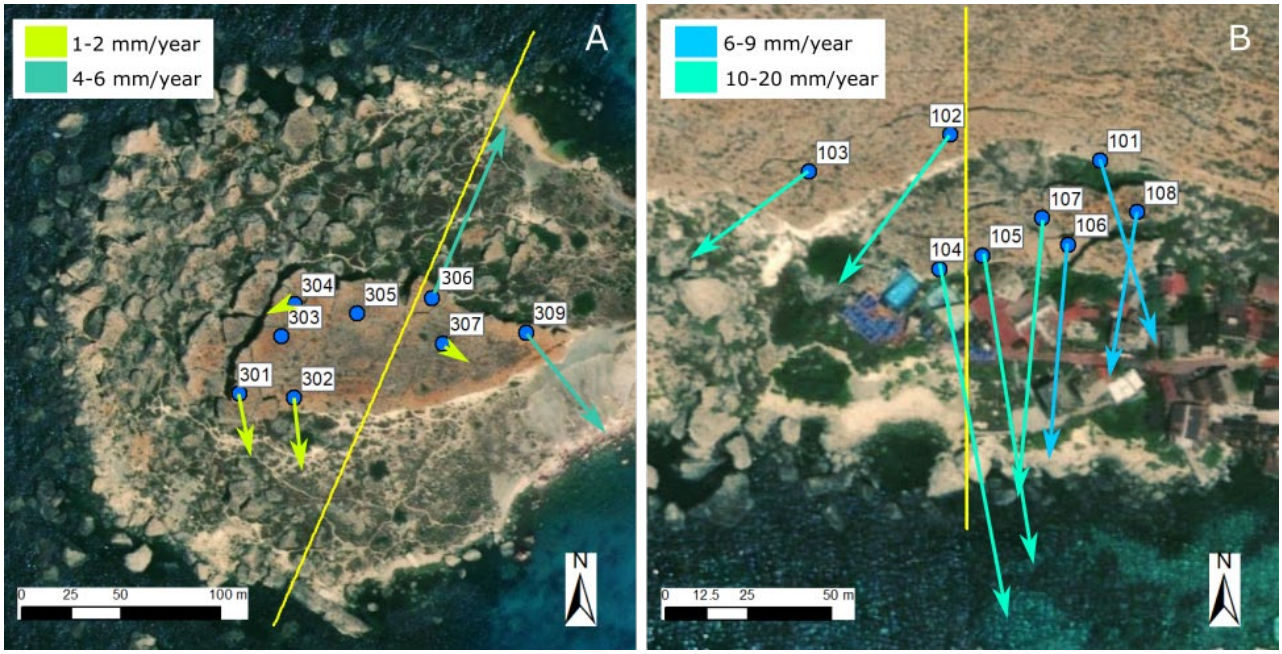

Figure 4. GNSS monitoring network and displacement vectors at Il-Qarraba (A) and Anchor Bay (B). The yellow lines represent the section used for the stability modelling.

Relative positioning requires simultaneous observations from at least two GNSS receivers, one at the reference station and the other at the unknown points. The accuracy in determining the positions of the monitoring benchmarks in the coordinate system depends on how well the error sources can be reduced. For example, long acquisition times at each measuring point indisputably improve the accuracy, but on the other hand there is always a trade-off limit between quality and costs. Considering the short baselines (Table 2), and thanks to extremely favorable conditions of sky

visibility due to the total absence of vegetation (i.e. trees), buildings and the modest presence of topographic relief, a 'fast static' survey procedure was considered acceptable.

Table 2. Baselines between the GNSS monitoring benchmarks and the reference station at the two test sites.

Test site	Maximum baseline length (m)	Average baseline length (m)
Il-Qarraba	504	449
Anchor Bay	357	300

For the measuring campaigns two geodetic (i.e. dual frequencies) GNSS receivers were employed. A detailed list of the parameters and processing technique adopted in the positioning of the monitoring benchmarks is summarized in Table 3.

Table 3. GNSS monitoring network processing parameters

Parameters	Values and Specifications
Acquisition time	20 min
Sampling rate	2 sec
Number of measurements	600
Cut off angle	15°
Tropospheric model	Hopfield
Positioning	Post-processing with precise ephemeris

3.1 GNSS Monitoring Results

The reliability of the displacements measured at each benchmark location is related to the positioning errors of the GNSS measurements. Typically, the accuracy of the planar components (i.e. Northings and Eastings) is similar, while the determination of the vertical component is more uncertain. For this reason, the computation of the displacements is often performed for these two components separately. In our analysis, the planar displacements were calculated by a vector combination of the Northing and Easting components, while the 3D displacements took into account also significant values (i.e. larger than the standard deviation) of vertical component

The displacements recorded at the two sites differ significantly in terms of magnitude and patterns. At Il-Qarraba, the survey benchmarks can be clustered into three groups according to style of activity and the magnitude of measured displacements. For points 303 and 305 these are seldom significant (i.e. the deformation vector is smaller than the error ellipses) and their patterns appear to be completely random, hence they are considered to be stable. For benchmarks 301, 302, 304 and 307 the displacement trend is less noisy although extremely slow, in the range 1-2 mm y^{-1}. The random patterns were interpreted as the effect of differential settlement of the Upper Coralline Limestone blocks over the Blue Clay (Figure 5). Finally, for points 306 and 309 a displacement trend is easily recognizable, having an estimated rate between 4-6 mm y^{-1} and consistent with a prevalent direction throughout the entire time series. All of the displacements recorded at the benchmarks are dominantly planar with minimal vertical components (Figure 6).

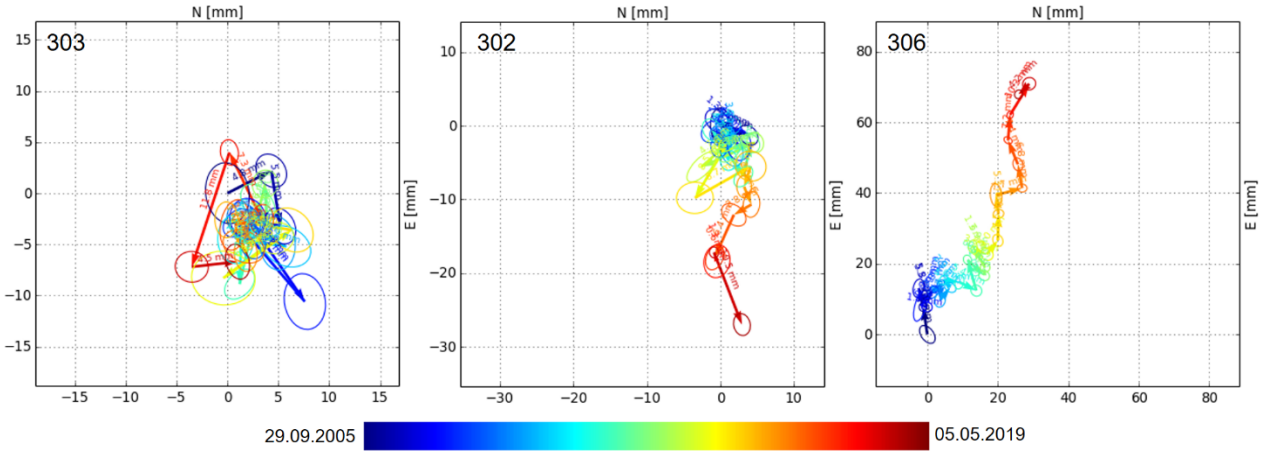

Figure 5. Displacement patterns of the most representative benchmark for each one of the three groups at Il-Qarraba. Error ellipses have a statistical significance level of 95%.

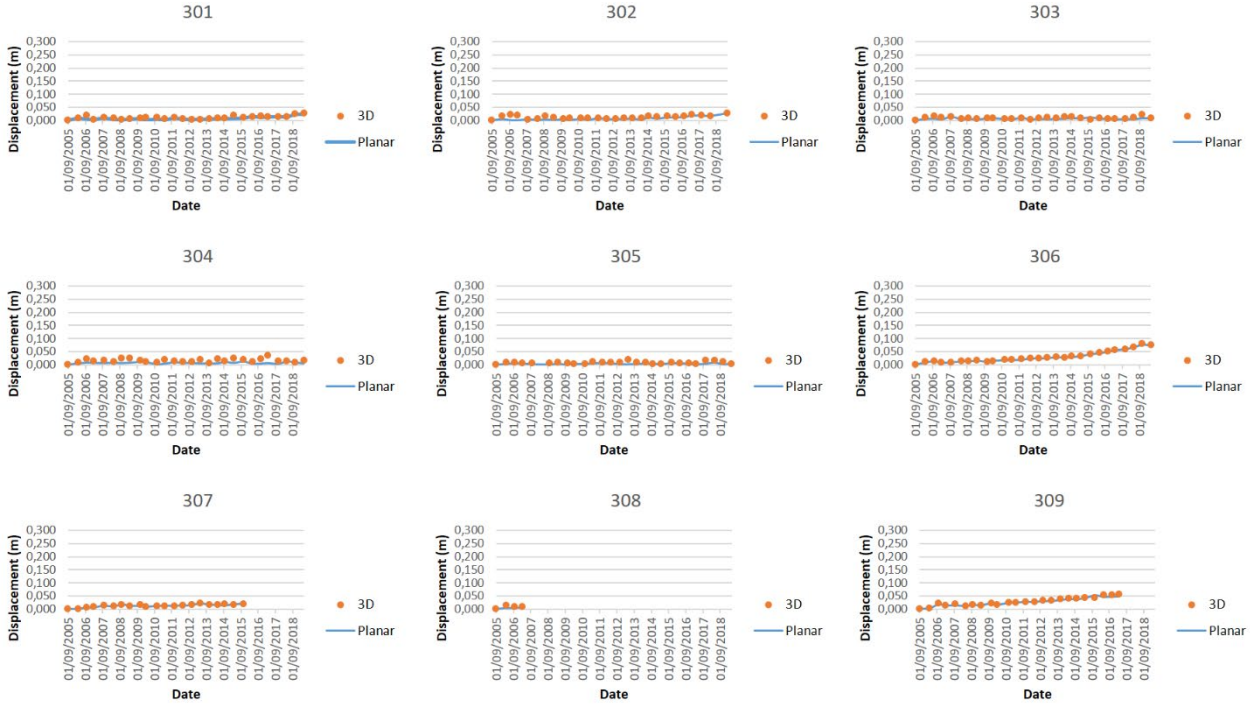

Figure 6. Planar (blue line) and 3D (orange dots) displacements recorded by the GNSS monitoring network at Il-Qarraba.

At Anchor Bay displacements are an order of magnitude higher compared with those at Il-Qarraba. Survey benchmarks 102, 103, 104, 105 and 107 move at an estimated rate of 10-20 mm y^{-1}. Unlike all the other monitoring points, the main component of the displacement is vertical at 102 and 103, consistent with the visible subsidence of the plateau affected by rock spreading (102 lowered by around 150 mm and 103 by more than 270 mm in 14 years). The movement rates of the remaining benchmarks 101, 106 and 108 varies between 6-9 mm y^{-1} (Figure 7). For all of the points at Anchor Bay a clear pattern of planar deformation towards the bay, although in slightly varying directions, can be identified.

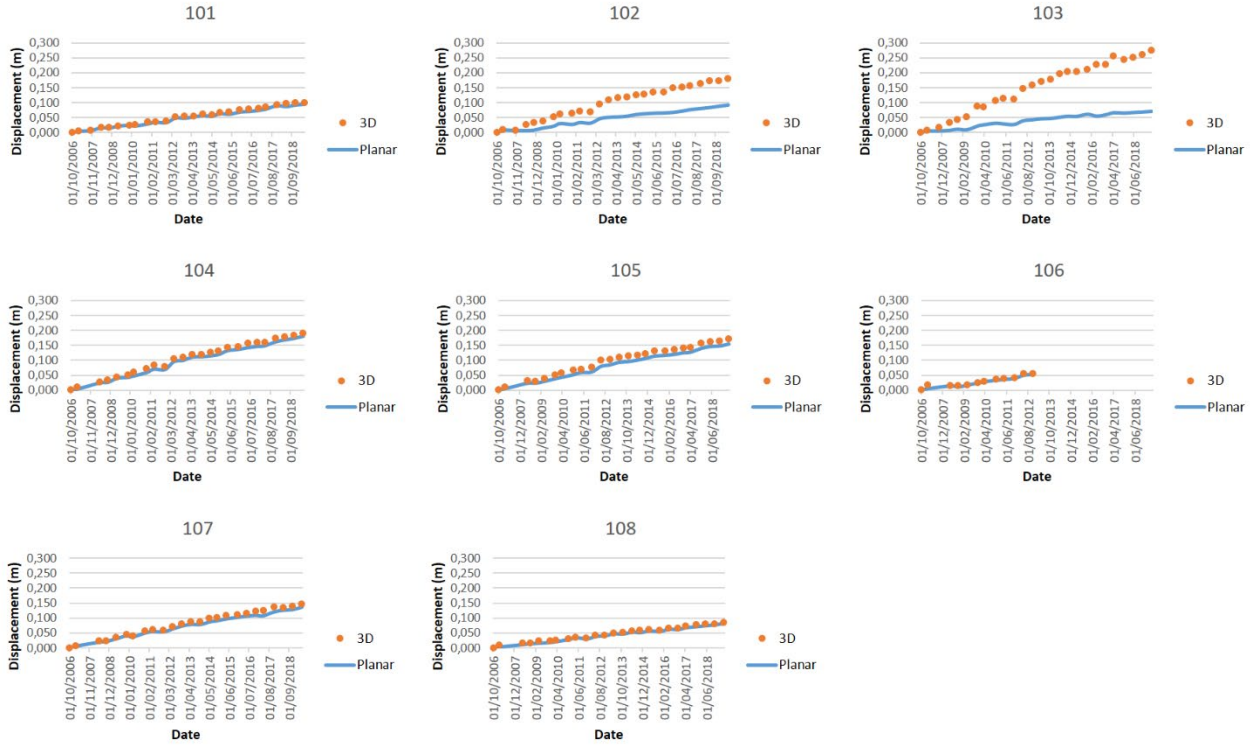

Figure 7. Planar (blue line) and 3D (orange dots) displacements recorded by the GNSS monitoring network at Anchor Bay. The subsidence recorded at benchmarks 102 and 103 is clear from the relative time-series.

4. Modelling

The point-like displacements patterns recorded by the GNSS monitoring system do not provide enough information for a comprehensive reconstruction of the landslide kinematics. In order to better understand the genesis and evolution of lateral spreading in rock, the identification of the predisposing instability factors and the governing failure mechanism(s) must be investigated. The long-term monitoring records can then be used to validate displacements obtained from the stability modelling. A two-dimensional model approach was considered appropriate, given the simple geometry of the coastal landslides, characterized by a single main slope direction and by uniform lateral constraints. The calculation strategy was implemented following a two-step process. Firstly, Limit Equilibrium Method (LEM) back-analyses were performed to determine probable values for the material properties, particularly the residual shear strength of the Blue Clay, using the fact that the Factor of Safety (FS) = 1.0 in slow-moving landslides at residual strength. The assumption that these properties were the same at both sites could also be tested by this method. Secondly, these derived material properties were then used with others estimated from the literature as inputs for the Finite Difference Model (FDM). The stability analyses were then validated by comparing the displacements calculated by the FDM with the GNSS records.

4.1 Limit Equilibrium Method

Although simple as a numerical approach, LEM was successfully applied to test the hypothesis that the different mechanical properties of the three materials (UCL, MM, BC) affected

by the mass movements were the same at both test sites. The mechanical parameters of the Upper Coralline Limestone and Mtarfa Member (Table 4) were derived from the geomechanical surveys conducted by Devoto (2013a), but the primary geological control on the landsliding is the Blue Clay. Basic geotechnical properties of this stiff overconsolidated clay were presented by Dykes (2002), supplemented by mineralogical analysis of Blue Clay from Marselforn in Gozo (Visser, 1991) that was assumed to apply throughout northwest Malta. From Dykes (2002), within 3 m of the surface this material has 'a strong massive structure interrupted by small irregular fissures' (p.82). It had a saturated unit weight of 19.6 kN m–3 (60% porosity) with 32% clay-sized particles, 67% silt (2-63 μm) and 2% sand (63-2000 μm). The measured index properties (plastic limit 30-32%, liquid limit 73-74%, plasticity index 41-44%, activity 1.3-1.4 and shrinkage 16-25%) were consistent with an indicative mineralogy (Visser, 1991) of 40% smectite, 35% kaolinite, 15% illite, 2-3% chlorite and 2-3% palygorskite. The stratigraphic position of the Blue Clay between thick limestones suggests calcium-based smectites, accounting for the relatively low activity, with the overall combination indicating a high-plasticity clay. Measured saturated hydraulic conductivity averaged 2×10^{-5} m s^{-1} but at the sampling depth the small fissures may have been the result of annual summer desiccation shrinkage and thus unrepresentative of the material at greater depths. Peak drained shear strength obtained from a 100 mm shearbox comprised an internal friction angle of 26.6° and cohesion of 4.5 kPa, which was found to be consistent with first-time shallow translational failures at Ghajn Tuffieha Bay (Dykes, 2002). The residual friction angle (Section 4.3.1) is higher than may be expected for smectite/illite rich clay but consistent with a significant kaolinite content and the high silt fraction (the above properties put the Blue Clay only just above the A-line).

Exploiting a 1 m resolution LiDAR DEM, one longitudinal section was selected for each site (see Figure 4). The profiles were chosen in accordance with the prevalent displacement direction calculated at the most active GNSS benchmarks locations. Geomorphological evidence was used to limit the search window for the scarp and the toe of each landslide. The LEM analysis was carried out using the Slide 5.0 software, assuming the Mohr-Coulomb failure criterion applied to all materials. The Morgenstern Price method (Morgenstern and Price, 1965) was used since it satisfies the equilibrium of both force and momentum (Duncan and Wright, 1980) and it provides results most comparable with advanced numerical methods (Griffiths and Lane, 1999; Liu at al., 2015). The section at Anchor Bay was analysed first, setting FS = 1.0 and using a non-circular path of search for a slip surface. Some judgement was used to assess whether any slip surface appeared realistic for a given set of material properties, but in fact the slip surface geometry was relatively insensitive to the shear strength values used. The material properties that gave FS = 1.0 were then used to analyse the Il-Qarraba section; obtaining FS ≈ 1 here would effectively validate those parameter values for use in the FDM stage

The modeling constraints were chosen based on two assumptions: (i) displaced blocks move on discrete shear surfaces (i.e. at residual shear strength), which was considered realistic considering the results of the long-term displacement monitoring data; (ii) the material properties are identical in both the study areas, based on the general geological and structural setting of the northwestern coast of Malta and the fact that the two test sites are less than 4 km apart. The mechanical parameters of the Upper Coralline Limestone and Mtarfa Member were derived from the geomechanical surveys conducted by Devoto (2013a), while the unit weight of the Blue Clay was assessed by laboratory analysis (Dykes, 2002). Under these approximations and assumptions, the only input parameter for the back -analysis was the residual friction angle of the Blue Clay (cohesion = 0 at residual strength). The water table level at Anchor Bay was determined basing on the geological and geotechnical characteristics of the main geological formations. Wells located further inland but in the proximity of the test sites usually record the presence of a water table at the contact between

Mtarfa Member and Blue Clay and that was considered the land-side boundary position. At Il-Qarraba, given the peculiar geometry of the promontory, the water table can be realistically assumed slightly above sea level.

4.2 Finite Differences Modelling

Once a single set of material properties has been derived that provides effectively FS = 1 for both of the study sites, particularly the residual friction angle for the Blue Clay, a FDM can be designed for both sites using the same soil parameters and keeping the Mohr–Coulomb elastic-plastic yield criterion for all the formations. The analysis was performed with the commercial software FLAC 6.0 (Fast Lagrangian Analysis of Continua), a well-established geotechnical model code from Itasca (Itasca, 2008) used in several landslides related applications (Quinn et al., 2010; Pasculli et al., 2018). In this modelling environment, the only additional soil parameters that would need some assumption/calibration are the elastic bulk modulus, the shear modulus and the tensile strength for the brittle formations. The criteria to validate the models are related to the consistency of modelled displacements with the data collected from the GNSS monitoring network. Specifically, the ratio between horizontal and vertical displacements of the monitoring benchmarks located along or close to the analysed sections are taken into consideration. The option to use the ratio instead of the absolute displacement values is justified since the model is time-independent (Bossi et al., 2019). The choice to apply a finite difference approach fits very well with the consideration that the main sliding mechanism of these slow-moving landslides is driven by the plastic Blue Clay, since a finite difference approach in a large strain framework is capable of reconstructing this kind of kinematic behavior. The scope of this model is, in fact, to match the monitoring data in order to assess a possible evolution of these landslides, rather than to consider the possible generation of retrogressive phenomena. The latter case would require a distinct element method code to reconstruct the development of the fractures and the cracking in the brittle Mtarfa Member and Upper Coralline Limestone formations during the first stage of instability (Gigli et al., 2012). Alternatively, in the proposed FLAC models, the presence of the main cracks is simulated through a local reduction of the tensile strength and cohesion of the brittle materials to reproduce the discontinuity.

4.3 Modelling Results

4.3.1 LEM analysis

At Anchor Bay, the analysed section runs in a N-S direction close to GNSS benchmarks 102 and 105. The scarp and toe limits for the search algorithm were imposed after field surveys while the solid Globigerina Limestone basement was assumed to be 10 m below the sea level (inferred from Prampolini et al., 2017, and Micallef et al., 2019). The mechanical properties of each formation used in the analysis are summarized in Table 4. The analysis produced FS = 0.989 using a residual friction angle of 16°, which is consistent with previously measured properties of the Blue Clay (Section 4.1).

Table 4. Material parameters used in the LEM model. γ = unit weight, φ = friction angle and c = cohesion. φ for the BC was obtained through back-analysis, the other values from laboratory tests.

Material	γ'(kN/m^3)	γ_{sat} (kN/m^3)	φ(deg.)	c (kN/m^2)
BC	16	19.6	16 (residual)	0 (residual)
MM	22	25	27	200
UCL	24.5	-	31	260

The shape of the slip surface is in good accordance with those expected for block slides (Figure 8). Several tests were carried out assuming different depths for the Globigerina Limestone basement, which is the parameter that carries the higher degree of uncertainty. Even in the most improbable scenarios (i.e. no GL basement), the FS stabilized around a value of 0.98 with a similar slip surface. The sensitivity of the calculated FS to the water table position within the slope was also tested and found to be low, i.e. the water table position had only a small influence, given the geometrical constraints.

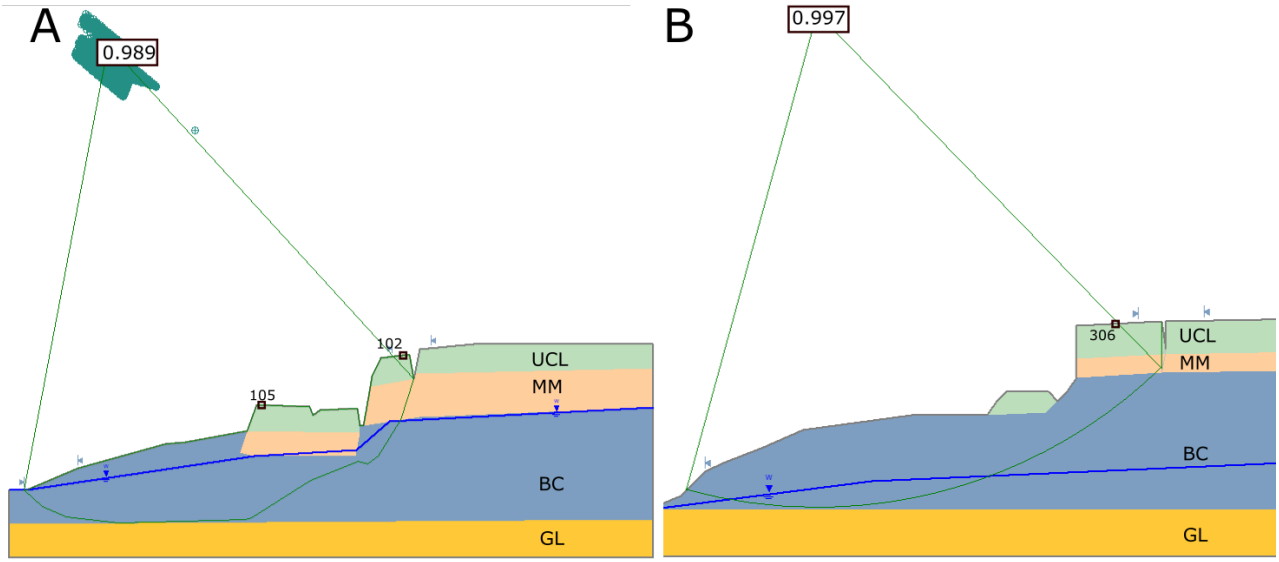

Figure 8. LEM modelling results for Anchor Bay (A) and Il-Qarraba (B).

An identical methodology with the same parameter values were then used for the analysed section at Il-Qarraba. Unlike for Anchor Bay, however, a circular surface option was selected due to the evidence of rotational movement shown by the detached blocks along the section. The result of the simulations provided FS = 0.997, thus validating the parameter values (Figure 9).

4.3.2 Finite Difference analysis

The Finite Difference models used the same geometries, densities and Mohr-Coulomb parameters as the LEM analysis. The elastic bulk modulus (K) and the shear modulus (G) for the brittle formations were estimated from data relating to similar lithological formations in scientific and technical literature (Palmström and Singh, 2001; Schön, 2011). In particular, for the UCL they are analogous to the values used for limestone in Alfaro et al (2019).

Regarding the tensile strength (TS), the slightly smaller values adopted for the UCL, compared with the Alfaro at al. (2019) values, is in accordance with Park and Michalowski (2017) that suggest reducing the TS for weathered rocks, such as the shallow coastal Maltese formations. Analogously, the TS of the MM (Q-value 0.8) was moderately reduced from the 10 kPa range proposed by Hoek and Brown (1997) for “very poor quality rock masses” (Table 5).

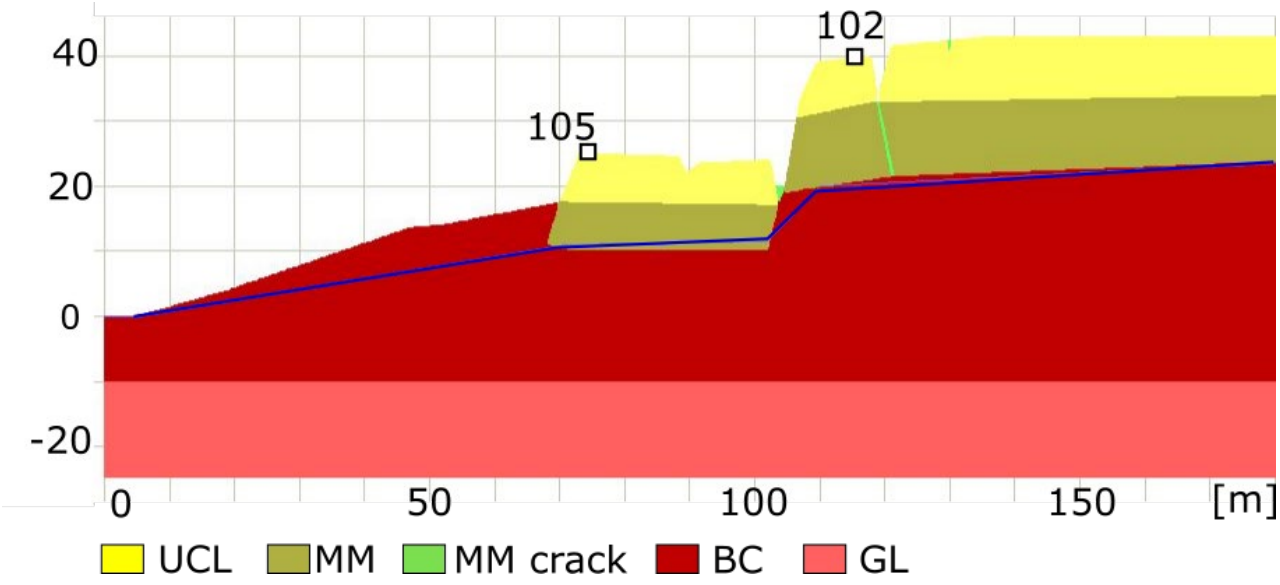

Figure 9. FLAC model for the Anchor Bay section.

Table 5. Additional material parameters used in FLAC: K = bulk modulus, G = shear modulus and TS = tensile strength.

Material	K (kPa)	G (kPa)	TS (kPa)
BC	$8.5 \cdot 10^5$	$2.5 \cdot 10^5$	0
MM	$2.68 \cdot 10^6$	$6.99 \cdot 10^5$	1.5
MM crack	$2.68 \cdot 10^6$	$6.99 \cdot 10^5$	0.1
UCL	$2.68 \cdot 10^7$	$6.99 \cdot 10^6$	150

The analysed section at Anchor Bay is characterized by the presence of a sub-vertical crack that cuts through the entire thickness of the Mtarfa Member layer (Mantovani et al., 2013; Devoto et al., 2020). The weakening effect of this was simulated through a reduction of the tensile strength and cohesion (20 kPa) of the Mtarfa Member crack in the FDM. An identical solution was used in a small area at the toe of the main cliff to simulate the loose debris accumulated after the displacement of the large detached block (Figure 9). It was decided to define specific "MM crack zones" rather than using the FLAC interface tool because of the relative thickness of these fissures, which are some meters wide, with respect to the size of the whole slope.

The results of the model show a very good agreement with the monitoring data (Table 6). The sliding dynamics comprise the plunging in the plastic formation of the frontal brittle portion of the cliff with consequent extrusion and sliding process in the Blue Clay (Figure 10).

Table 6. Displacement comparison between monitoring data and modelled results for the Anchor Bay section.

Benchmark	X disp. (m)	Y disp. (m)	Ratio X disp./Y disp.
102 GNSS	-0.073	-0.154	0.474
102 model	-0.039	-0.069	0.568 (19% error)
105 GNSS	-0.153	-0.069	2.219
105 model	-0.080	-0.034	2.323 (5% error)
Ratio 102/105 GNSS	0.477	2.233	
Ratio 102/105 model	0.478 (2% error)	1.991 (11% error)	

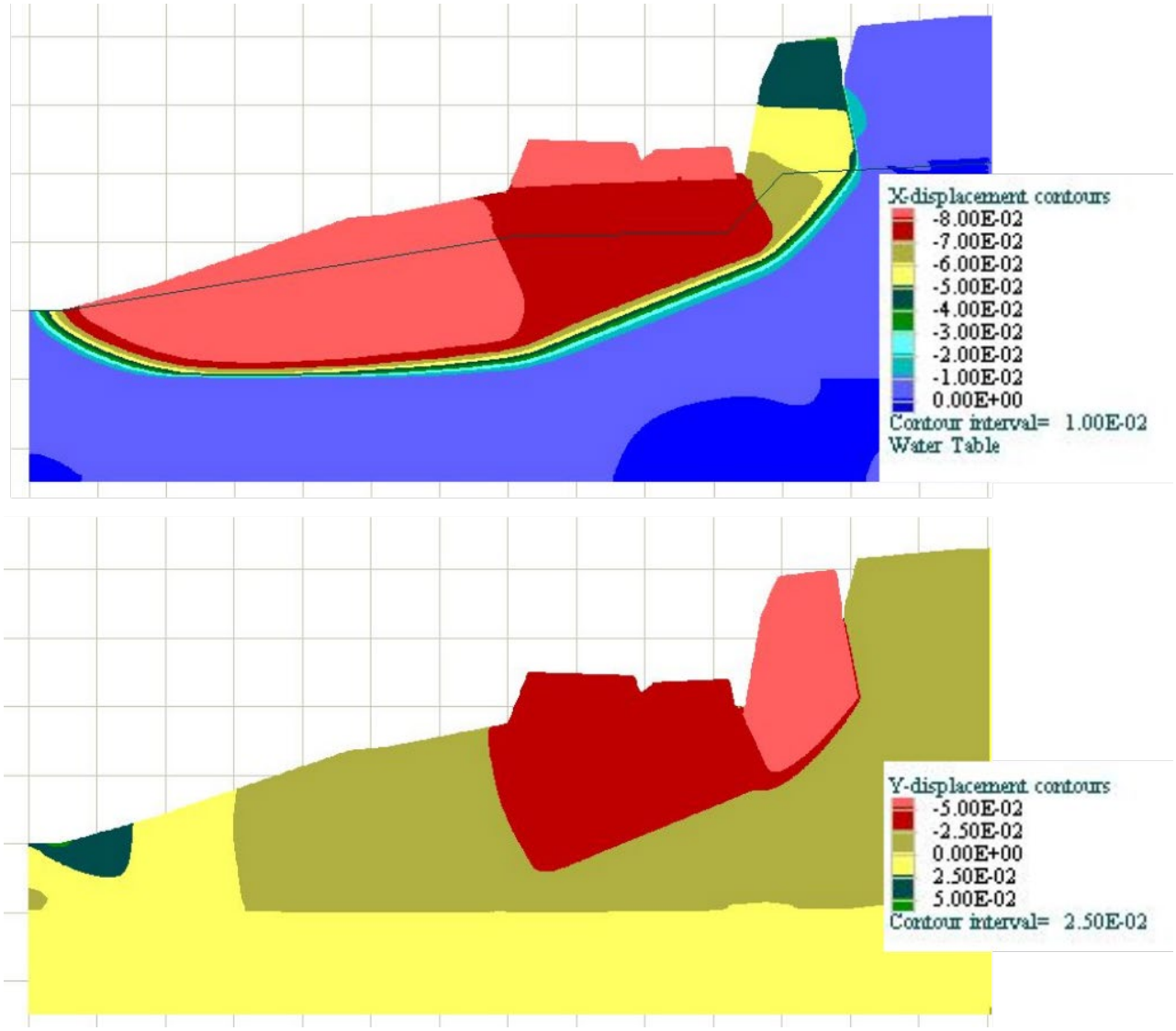

Figure 10. Displacements in the horizontal and vertical direction in the Anchor Bay section.

The Il-Qarraba section is characterized by a vertical tension crack behind the scarp and the presence of several Upper Coralline Limestone boulders scattered around the slope (Devoto et al., 2020), mainly on the shoreline and at the toe of the cliff (Figure 11). The model results are congruent with the displacements recorded at measurement point 306. Along this analysed section the presence of Upper Coralline Limestone boulder, just below the cliff, profoundly influences the kinematics of the rock spread. In fact, the simulated displacements would not have corresponded with those recorded at survey benchmark 306 if this boulder had not been included in the model (Table 7). On the contrary, through the incorporation of the boulder, three superimposed slip surfaces are generated. The first one is located just below the caprock cliff, inducing toppling, the second runs in the Blue Clay parallel to the topographic surface halfway up the slope, and the third, the deepest, has a similar shape to the one modelled at Anchor Bay (Figure 12).

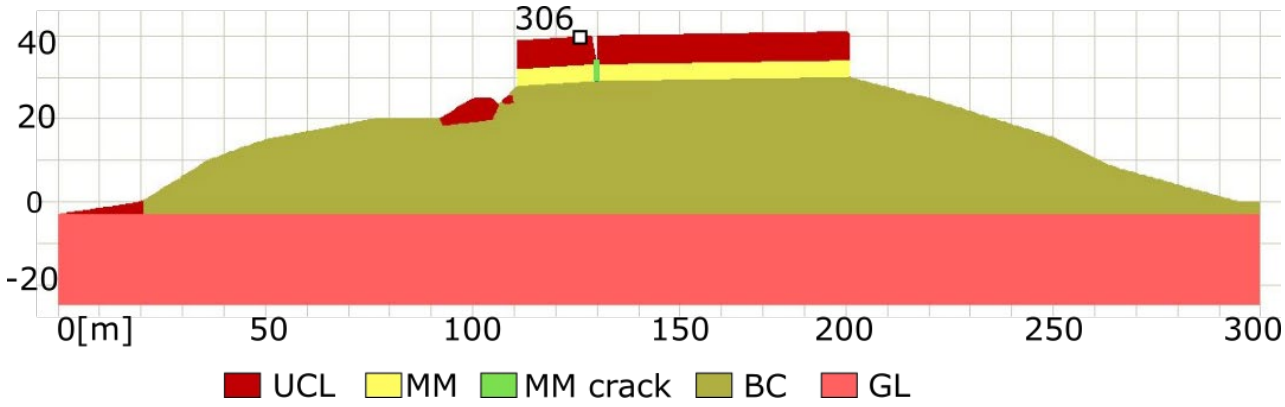

Figure 11. FLAC model for the Il-Qarraba section.

Table 7. Displacement comparisons between monitoring data and modelled results for the Il-Qarraba section.

Benchmark	X disp. (m)	Y disp. (m)	Ratio X disp./Y disp.
306 GNSS	-0.073	-0.019	3.88
306 model with boulder	-0.153	-0.041	3.69 (5% error)
306 model without boulder	-0.263	-0.055	4.82 (24% error)

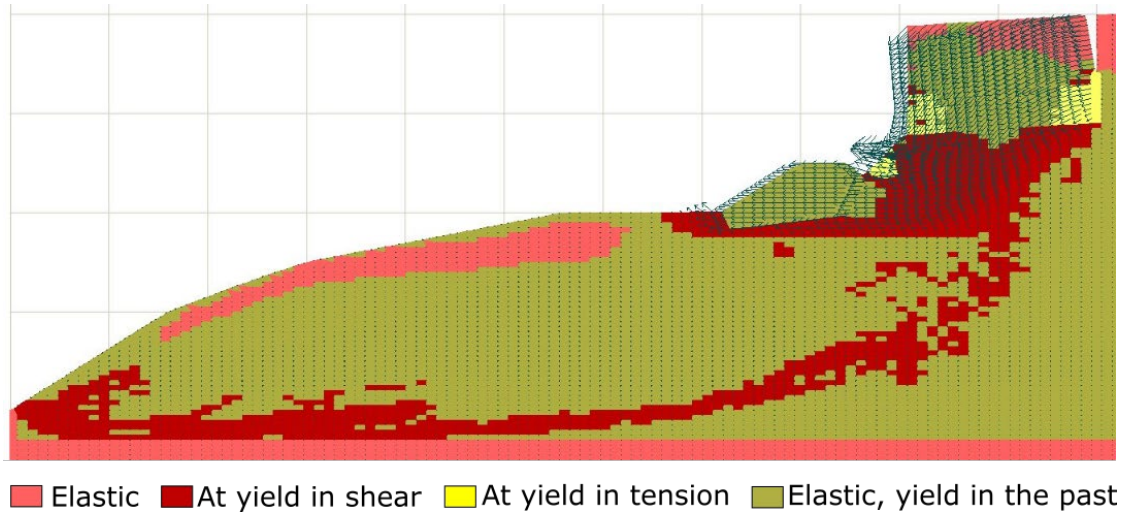

Figure 12. Displacement vectors and plasticity zones in the Il-Qarraba model: enlargement of the northern and most active part of the modelled section

5. Discussion

The aim of this study was to determine whether the stability and failure conditions of rock spreads could be established through long term monitoring providing the means of validating numerical models. In this work, a 14 years long GNSS monitoring campaign was performed over two rock spreads located in the northwestern coast of the island of Malta. This exceptionally long monitoring record served as calibrating and validating data for the numerical modelling (Limit Equilibrium Method and Finite Difference Model) through which the failure mechanism of the landslides was investigated. The modeled landslide kinematics provided convincing explanations to the different displacement patterns observed at the sections of the two test sites.

Modelled displacements of large blocks of rock within two zones of active lateral spreading correspond with measurements obtained from the long-term GNSS monitoring campaign in terms of the ratio of horizontal to vertical movements. In common with some other studies of lateral spreads in rock (e.g. Delgado et al., 2011), it is not yet known whether these mass movements are founded on discrete shear surfaces or whether they involve zones of ductile deformation – although Panzera et al. (2012) suggested that the outputs of seismic data were showing a distinct basal sliding surface of displaced material over Blue Clay near the village of Xemxija in northeast Malta.

The modeled landslide movements accurately characterized the subsidence of the edge of the plateau and the consequent quasi-planar slide of the cracked unit at Anchor Bay, although the FD analysis slightly under-represented the vertical subsidence of the upper block. Previous studies of lateral spreading failures in rock using both analogue and numerical modelling techniques have shown that the rheology of the ductile material needed to change over time for this type of mass movement to fully develop (Bozzano et al., 2013; Bois et al., 2018). The results from Malta so far suggest that the Mohr–Coulomb elastic-plastic yield criterion probably applies within established failures, although conditions for initiation of these failures have not yet been investigated. Mantovani et al. (2013) previously established that the base of the BC on the GL has a planar dip towards the SSE at Anchor Bay, which may influence the development of the main block sliding phase of the landslide, but toppling of the large upper block (benchmark 102) – as observed elsewhere (e.g. Tomás et al., 2018) – is unlikely to occur because it is supported by the very large downslope block.

At Il-Qarraba, the presence of three deformation bands or zones indicated by the FD model requires examination. The first zone, located just below the rocky cliff, does induce toppling of the block detached from the plateau. Evidence of toppling can be found in many of the boulders scattered around the slope along the line of the modeled section. The second one is horizontal and cutting just below the boulders. It causes the planar displacement measured by benchmark 306 and, by emerging halfway in the Blue Clay formation, it explains the clear reduction in the inclination of the slope along the section. Finally, the deepest band has a shape similar to the one modelled at Anchor Bay but its influence on the overall kinematics is lower as the toppling mechanisms further upslope dominates the slope development. The presence of these multiple sliding surfaces explains the differences in the kinematic behavior between the two sites as recorded by the GNSS data.

At both of the study sites, the deposition zone for limestone blocks separated from the escarpment edges by lateral spreading and block slides extends for considerable distances down the gently inclined slopes that now constitute the sea bed below present sea level (Prampolini et al., 2017; Soldati et al., 2018). Soldati et al. (2018) concluded from dating evidence that these landslide systems probably involved large-scale failure events (rock spreads) with subsequent breakdown of the larger displaced blocks by falls and topples to produce the numerous small sliding blocks visible today. The smaller sliding blocks – which may still be of considerable size, e.g tens of metres in length (Devoto et al., 2020) – not only armour the slopes below the current headscar cliffs against marine erosion but must have likewise protected the GL and the lower BC from the last ~40 m of post-LGM sea level rise. Furthermore, the failure at Anchor Bay must extend almost as deep as the GL contact at the base of the BC. It therefore seems possible that the major rock spreads visible today are, in fact, the remains of the first to have occurred at each site.

A major hazard of some lateral rock spreads is that they could catastrophically accelerate and collapse (Ietto et al., 2015; Mateos et al., 2018) but this requires them to have formed along plateau edges on the upper parts of high, steep slopes. In this type of topographic context either the front part of a spreading failure or an entire sliding mass could create a highly damaging rapid debris avalanche. Fortunately this scenario does not arise on Malta, where all the lateral spreads and

associated block slides are located on relatively low (elevation and gradient) slopes, becoming significantly less steep below sea level. If these mass movements are all assumed to be seated in clay at residual strength, i.e. FS = 1, then they are essentially at equilibrium and only move in response to the balance of forces being changed – either increasing the disturbing force or, more likely, reducing the resisting force – sufficiently to overcome the prevailing friction and inertia so as to allow movement. If the movement occurs primarily by means of ductile or plastic deformations within a zone of remoulded clay, the same general argument applies.

The hazards associated with the active rock spreads and block slides on Malta might be, in some settings, potentially severe. Tomás et al. (2018, p.241) wrote: '*it is well known that despite the low displacement rate of rock spreadings, they can induce hazardous, collateral, faster landslides as topples and rockfalls, mainly on edges of the mobilized rock mass that are not confined laterally*', which applies here. There is abundant evidence of small rock falls and topples occurring in the past from the headscar cliffs as well as the downslope faces of displaced limestone blocks within all of northwest Malta's landslide zones. One of the open questions was whether these toppling phenomena may be possible given the present characteristics and conditions of these coastal sites. In terms of exposed elements, most of these zones are generally inaccessible although a few of these locations are regularly visited by locals and tourists alike. Anchor Bay is the site of primary concern from the risk assessment point of view. The large blocks that comprise the rock spreads do not constitute a hazard but these slow movements may cause, or allow, additional cracks to form within those blocks due to flexural stresses leading to small rock falls or topples that could cause fatalities. Periodic surveys focused on the identification of new cracks along with monitoring should therefore be performed to update the hazard scenario if needed be. On the other hand, tourists following the footpaths round the isthmus often visit Il-Qarraba. The modelling results show that the expected evolution of this site may involve toppling providing a certain degree of risk for passing by excursionists.

6. Conclusions

A very long record of displacement data combined with very detailed topographical information have made it possible to analyse representative cross-sections through two lateral spreading mass movements and to validate the displacements simulated by the Finite Difference Model. The FDM results show zones of deformation through the Blue Clay consistent with the geometries of slip surfaces obtained by Limit Equilibrium back-analyses, and produced patterns of displacement consistent with measurements. As such, they suggest that the deformation of the BC is controlled by the Mohr–Coulomb elastic-plastic yield criterion. This conclusion applies only to these fully-developed landslides: nothing can be said about the conditions causing initial cracking of the Upper Coralline Limestone caprock.

It is not known whether these rock spreads move by basal sliding on a shear surface at residual strength or by ductile deformation of a band of the Blue Clay (or some combination of both mechanisms), but the FDM results do explain differences in the measured patterns of displacement at the two study sites. As such, this modelling approach appears to provide a means of assessing the nature of any hazard at the other rock spreading sites on Malta, in particular to identify locations where topples may be likely to occur in the future. In addition to improving the hazard assessments, it should be possible to forecast evolutionary scenarios for all of Malta's coastal lateral spreading landslides.

Lastly, the large degree of uncertainties makes a reliable assessment of the lateral spreading hazard by means of modelling rather difficult to achieve, even though some of these phenomena may evolve into faster movements. In Malta, however, the usual major sources of uncertainty are highly reduced. In fact, there are not strong variations of the water table location, the discontinuities are sub-vertical and the layering horizontal. Besides, a constant and uniform slope topography permits two-dimensional modelling. The simplicity of the setting of the northwestern coast of Malta makes it a perfect case study for lateral spreading and associated mass movements.

Acknowledgments

The research is also part of the Project "Coastal risk assessment and mapping" funded by the EUR-OPA Major Hazards Agreement of the Council of Europe (2020–2021). Grant Number: GA/2020/06 n◦ 654503 (Unimore Unit Resp.: Mauro Soldati).

References

Agnesi, V., Rotigliano, E., Tammaro, U., Cappadonia, C., Conoscenti, C., Obrizzo, F., Di Maggio, C., Luzio, D., Pingue, F., 2015. GPS Monitoring of the Scopello (Sicily, Italy) DGSD Phenomenon: Relationships Between Surficial and Deep-Seated Morphodynamics, in: Lollino, G., Giordan, D., Crosta, G.B., Corominas, J., Azzam, R., Wasowski, J., Sciarra, N. (Eds.), Engineering Geology for Society and Territory – Volume 2. Springer, Cham, pp. 1321-1325. https://doi.org/10.1007/978-3-319-09057-3_232.

Alfaro, P., Delgado, J., Esposito, C., García-Tortosa, F., Marmoni, G.M., Martino, S., 2019. Time-dependent modelling of a mountain front retreat due to a fold-to-fault controlled lateral spreading. Tectonophysics 773, 228233. https://doi.org/10.1016/j.tecto.2019.228233.

Angeli, M.-G., Pasuto, A., Silvano, S., 2000. A critical review of landslide monitoring experiences. Engineering Geology 55 (3), 133–147. https://doi.org/10.1016/S0013-7952(99)00122-2.

Arosio, D., Longoni, L., Papini, M., Bièvre, G., Zanzi, L., 2019. Geological and geophysical investigations to analyse a lateral spreading phenomenon: the case study of Torrioni di Rialba, northern Italy. Landslides 16, 1257-1271. https://doi.org/10.1007/s10346-017-0865-0.

Bois, T., Zerathe, S., Lebourg, T., Tric, E., 2018. Analysis of lateral rock spreading process initiation with a numerical modelling approach. Terra Nova 30, 369-379. https://doi.org/10.1111/ter.12352

Bossi, G., Borgatti, L., Gottardi, G., Marcato G., 2019. Quantification of the uncertainty in the modelling of unstable slopes displaying marked soil heterogeneity. Landslides 16, 2409–2420. https://doi.org/10.1007/s10346-019-01256-x.

Bounab, A., El Kharim, Y., El Hamdouni, R., Hlila, R., 2021. A multidisciplinary approach to study slope instability in the Alboran Sea shoreline: Study of the Tamegaret deep-seated slow-

moving landslide in Northern Morocco. Journal of African Earth Sciences 184, 104345. https://doi.org/10.1016/j.jafrearsci.2021.104345.

Bozzano, F., Bretschneider, A., Esposito, C., Martino, S., Prestininzi, Scarascia Mugnozza, G., 2013. Lateral spreading processes in mountain ranges: Insights from an analogue modelling experiment. Tectonophysics 605, 88-95. https://doi.org/10.1016/j.tecto.2013.05.006

Carobene, L., Cevasco, A., 2011. A large scale lateral spreading, its genesis and Quaternary evolution in the coastal sector between Cogoleto and Varazze (Liguria — Italy). Geomorphology 129, 398-411. https://doi.org/10.1016/j.geomorph.2011.03.006.

Casagli, N., Frodella, W., Morelli, S., Tofani, V., Ciampalini, A., Intrieri, E., Raspini, F., Rossi, G., Tanteri, L., Lu, P., 2017. Spaceborne, UAV and ground-based remote sensing techniques for landslide mapping, monitoring and early warning. Geoenvironmental Disasters 4:9. https://doi:10.1186/s40677-017-0073-1.

Coe, J.A., Ellis, W.L., Godt, J.W., Savage, W.Z., Savage, J.E., Michael, J.A., Kibler, J.D., Powers, P.S., Lidke, D.J., Debray, S., 2003. Seasonal movement of the Slumgullion landslide determined from Global Positioning System surveys and field instrumentation, July 1998-March 2002. Engineering Geology 68, 67–101. https://doi.org/10.1016/S0013-7952(02)00199-0.

Colesanti, C., Wasowski, J., 2006. Investigating Landslides with Space-Borne Synthetic Aperture Radar (SAR) Interferometry. Engineering Geology 88, 173-199. https://doi.org/10.1016/j.enggeo.2006.09.013

Corsini, A., Pasuto, A., Soldati, M., Zannoni, A., 2005. Field monitoring of the Corvara landslide (Dolomites, Italy) and its relevance for hazard assessment. Geomorphology 66, 149-165. https://doi.org/10.1016/j.geomorph.2004.09.012.

Cruden, D.M., Varnes, D.J., 1996. Landslide types and processes. In: Turner, A.K., Schuster, R.L., (Eds.), Landslides: Investigation and Mitigation, Transp. Res. Board, Spec. Rep., vol. 247. National Academy Press, Washington, D.C., pp. 36-75.

Delgado, J., Vicente, F., García-Tortosa, F., Alfaro, P., Estévez, A., Lopez-Sanchez, J.M., Tomás, R., Mallorquí, J.J., 2011. A deep seated compound rotational rock slide and rock spread in SE Spain: Structural control and DInSAR monitoring. Geomorphology 129, 252-262. https://doi.org/10.1016/j.geomorph.2011.02.019

Della Seta, M., Martino, S., Scarascia Mugnozza, G., 2013. Quaternary sea-level change and slope instability in coastal areas: Insights from the Vasto Landslide (Adriatic coast, central Italy). Geomorphology 201, 462-478. https://doi.org/10.1016/j.geomorph.2013.07.019.

Devoto, S., Biolchi, S., Bruschi, V.M., Furlani, S., Mantovani, M., Piacentini, D., Pasuto, A., Soldati, M., 2012. Geomorphological map of the NW Coast of the Island of Malta. Journal of Maps 8, 33-40. https://doi.org/10.1080/17445647.2012.668425

Devoto, S. 2013a. Cartografia, monitoraggio e modellizzazione di frane lungo la costa nord-occidentale dell'isola di Malta. Ph.D. Thesis, University of Modena and Reggio Emilia,

608 Modena, 03 April 2013.

609 Devoto, S., Biolchi, S., Bruschi, V.M., Gonzalez Diez, M., Mantovani, M., Pasuto, A., Piacentini,
610 D., Schembri, J.A., Soldati, M., 2013b. Landslides along the north-west coast of the Island of
611 Malta, in: Margottini C, Canuti P, Sassa K. (Eds.), Landslide Science and Practice - Volume 1:
612 Landslide Inventory and Susceptibility and Hazard Zoning. Springer-Verlag, Berlin
613 Heidelberg, pp. 57-63. https://doi.org /10.1007/978-3-642-31325-7-7.

614 Devoto, S., Macovaz, V., Mantovani, M., Soldati, M., Furlani, S., 2020. Advantages of Using
615 UAV Digital Photogrammetry in the Study of Slow-Moving Coastal Landslides. Remote
616 Sensing 12, 3566. https://doi.org/10.3390/rs12213566.

617 Devoto, S., Hastewell, L.J., Prampolini, M., Furlani, S., 2021. Dataset of Gravity-Induced
618 Landforms and Sinkholes of the Northeast Coast of Malta (Central Mediterranean Sea). Data,
619 6, 81. https://doi.org/10.3390/data6080081.

620 Di Martire, D., Novellino, A., Ramondini, M., Calcaterra, D, 2016. A-Differential Synthetic
621 Aperture Radar Interferometry analysis of a Deep Seated Gravitational Slope Deformation
622 occurring at Bisaccia (Italy). Science of the Total Environment 550, 556-573.
623 https://doi.org/10.1016/j.scitotenv.2016.01.102.

624 Dykes, A.P., 2002. Mass movements and conservation management in Malta, Journal of
625 Environmental Management 66(1), 77-89. https://doi.org/10.1006/jema.2002.0577.

626 Duncan, J. M., Wright, S.G., 1980. The accuracy of equilibrium methods of slope stability
627 analysis. Engineering Geology 16(1-2), 5-17. https://doi.org/10.1016/0013-7952(80)90003-4

628 Fiorillo, F., 2003. Geological features and landslide mechanisms of an unstable coastal slope
629 (Petacciato, Italy). Engineering Geology 67, 255–267. https://doi.org/10.1016/S0013-
630 7952(02)00184-9.

631 Galea, P., 2019. Central Mediterranean Tectonics—A Key Player in the Geomorphology of the
632 Maltese Islands, in: Gauci, R., Schembri, J. (Eds.), Landscapes and Landforms of the Maltese
633 Islands. World Geomorphological Landscapes. Springer, Cham, pp. 19-30.
634 https://doi.org/10.1007/978-3-030-15456-1_14.

635 Gauci R., Scerri, S., 2019. A Synthesis of Different Geomorphological Landscapes on the Maltese
636 Islands, in: Gauci, R., Schembri, J. (Eds.), Landscapes and Landforms of the Maltese Islands.
637 World Geomorphological Landscapes. Springer, Cham, pp. 49-65. https://doi.org/10.1007/978-
638 3-030-15456-1_14.

639 Gigli, G., Frodella, W., Mugnai, F., Tapete, D., Cigna, F., Fanti, R., Intrieri, E., Lombardi, L.,
640 2012. Instability mechanisms affecting cultural heritage sites in the Maltese Archipelago.
641 Natural Hazards and Earth System Science 12 (6). 1883-1903. https://doi.org/10.5194/nhess-
642 12-1883-2012.

643 Gili, J.A., Corominas, J., Rius, J., 2000. Using Global Positioning System techniques in landslide
644 monitoring. Engineering Geology 55 (3), 167–192. https://doi:10.1016/s0013-7952(99)00127-
645 1.

Griffiths, D.V., Lane, P. A., 1999. Slope stability analysis by finite elements. Geotechnique 49(3), 387-403. https://doi.org/10.1680/geot.1999.49.3.387.

Hoek, E. and Brown, E.T., 1997. Practical estimates of rock mass strength. International journal of rock mechanics and mining sciences, 34(8), 1165-1186.

Hofman-Wellenhof, B., Lichtenegger, H., Collins, J., 2001. GPS - Theory and Practice, Fifth revisited ed., Springer-Verlag, Wien New York. ISBN 3-211-83534-2.

Kirschbaum, D.B., Adler, R., Hong, Y., Hill, S., Lerner-Lam, A., 2010. A global landslide catalog for hazard applications: method, results, and limitations. Natural Hazards 52, 561-575. https://doi.org/10.1007/s11069-009-9401-4.

Ietto, F., Perri, F., Fortunato, G., 2015. Lateral spreading phenomena and weathering processes from the Tropea area (Calabria, southern Italy). Environmental Earth Sciences 73, 4595–4608. https://doi.org/10.1007/s12665-014-3745-0

Ilia, I., Koumantakis, I., Rozos, D., Koukis, G., Tsangaratos, P., 2015. A Geographical Information System (GIS) Based Probabilistic Certainty Factor Approach in Assessing Landslide Susceptibility: The Case Study of Kimi, Euboea, Greece, in: Lollino, G., Giordan, D., Crosta, G.B., Corominas, J., Azzam, R., Wasowski, J., Sciarra, N. (Eds.), Engineering Geology for Society and Territory – Volume 2. Springer, Cham, pp. 1199-1204. https://doi.org/10.1007/978-3-319-09057-3_210.

Itasca Consulting Group (2008) FLAC 6.0 - user manual. Itasca Consulting Group Inc., Minneapolis, Minnesota.

Lacroix, P., Handwerger, A. L., Bievre, G., 2020. Life and death of slow-moving landslides. Nature Reviews Earth & Environment 1, 404–419. https://doi.org/10.1038/s43017-020-0072-8

Liu, S.Y., Shao, L.T., Li, H.J., 2015. Slope stability analysis using the limit equilibrium method and two finite element methods. Computers and Geotechnics 63, 291-298. https://doi.org/10.1016/j.compgeo.2014.10.008

Malet, J.-P., Maquaire, O., Calais, E., 2002. The use of Global Positioning System techniques for the continuous monitoring of landslides: application to the Super-Suaze earthflow (Alpes-de-Haute-Provence, France). Geomorphology 43, 33-54. https://doi.org/10.1016/S0169-555X(01)00098-8.

Mansour, M.F., Morgenstern, N.R., Martin, C.D., 2011. Expected damage from displacement of slow-moving slides. Landslides 8, 117-131. https://doi.org/10.1007/s10346-010-0227-7.

Mantovani, M., Bossi, G., Marcato, G., Schenato, L., Tedesco, G., Titti, G., Pasuto, A., 2019. New Perspectives in Landslide Displacement Detection Using Sentinel-1 Datasets. Remote Sensing 11, 2135. https://doi.org/10.3390/rs11182135

Mantovani, M., Devoto, S., Forte, E., Mocnik, A., Pasuto, A., Piacentini, D., Soldati, M., 2013. A multidisciplinary approach for rock spreading and block sliding in the north-western coast of Malta. Landslides, 10, 611-622. https://doi.org/10.1007/s10346-012-0347-3

683 Mantovani, M., Devoto, S., Piacentini, D., Prampolini, M., Soldati, M., Pasuto, A., 2016.
684 Advanced SAR interferometric analysis to support geomorphological interpretation of slow-
685 moving coastal landslides (Malta, Mediterranean Sea). Remote sensing 8(6),
686 443. https://doi.org/10.3390/rs8060443.

687 Mariani, G.S., Zerboni, A., 2020. Surface Geomorphological Features of Deep-Seated
688 Gravitational Slope Deformations. Geosciences 10, 334.
689 https://doi.org/10.3390/geosciences10090334.

690 Mateos, R.M., Ezquerro, P., Azañón, J.M., Gelabert, B., Herrera, G., Fernández-Merodo, J.A.,
691 Spizzichino, D., Sarro, R., Garcia-Moreno, I., Bejar-Pizarro, M., 2018. Coastal lateral
692 spreading in the world heritage site of the Tramuntana Range (Majorca, Spain). The use of
693 PSInSAR monitoring to identify vulnerability. Landslides 15, 797–809.
694 https://doi.org/10.1007/s10346-018-0949-5.

695 Miccadei, E., Mascioli, F., Ricci, F., Piacentini, T., 2019. Geomorphology of soft clastic rock
696 coasts in the mid-western Adriatic Sea (Abruzzo, Italy). Geomorphology 324, 72-94.
697 https://doi.org/10.1016/j.geomorph.2018.09.023.

698 Micallef, A., Spatola, D., Caracausi, A., Italiano, F., Barreca, G., D'Amico, S., Petronio, L., Coren,
699 F., Facchin, L., Blanos, R., Pavan, A., Paganini, P., Taviani, M., 2019. Active degassing across
700 the Maltese Islands (Mediterranean Sea) and implications for its neotectonics. Marine and
701 Petroleum Geology 104, 361–374. https://doi.org/10.1016/j.marpetgeo.2019.03.033

702 Morgenstern, N.R., Price, V.E., 1965. The analysis of the stability of general slip surfaces.
703 Geotechnique 15 (1), 79-93. https://doi.org/10.1680/geot.1965.15.1.79

704 Palis, E., Lebourg, T., Tric, E., Malet J.-P., Vidal, M., 2017. Long-term monitoring of a large
705 deep-seated landslide (La Clapiere, South-East French Alps): initial study. Landslides 14, 155–
706 170. https://doi.org/10.1007/s10346-016-0705-7.

707 Pánek, T., Klimeš, J., 2016. Temporal behavior of deep-seated gravitational slope deformations: A
708 review. Earth-Science Reviews 156, 14-38. https://doi.org/10.1016/j.earscirev.2016.02.007

709 Panzera, F., D'Amico, S., Lotteri, A., Galea, P., Lombardo, G., 2012. Seismic site response of
710 unstable steep slope using noise measurements: the case study of Xemxija Bay area, Malta.
711 Natural Hazards and Earth System Science 12, 3421-3431. https://doi.org/10.5194/nhess-12-
712 3421-2012

713 Palmström, A., Singh, R., 2001. The deformation modulus of rock masses—comparisons between
714 in situ tests and indirect estimates. Tunnelling and Underground Space Technology, 16(2), pp.
715 115-131.

716 Park, D., Michalowski, R. L., 2017. Three-dimensional stability analysis of slopes in hard soil/soft
717 rock with tensile strength cut-off. Engineering Geology, 229, 73-84.

718 Pasculli, A., Calista, M., Sciarra, N., 2018. Variability of local stress states resulting from the
719 application of Monte Carlo and finite difference methods to the stability study of a selected
720 slope. Engineering Geology. 245, 370-389. https://doi.org/10.1016/j.enggeo.2018.09.009

721 Pasuto, A, Soldati, M., 2013. Lateral spreading. In: Shroder JF, Marston RA, Stoffel M (Eds.)
722 Treatise on geomorphology, vol 7. Mountain and Hillslope geomorphology. Academic Press,
723 San Diego, pp. 239–248

724 Petley, D.N., Mantovani, F., Bulmer, M.H., Zannoni, A., 2005. The use of surface monitoring data
725 for the interpretation of landslide movement patterns. Geomorphology 66, 133-147.
726 https://doi.org/10.1016/j.geomorph.2004.09.011.

727 Peyret, M., Djamour, Y., Rizza, M., Ritz, J.-F., Hurtrez, J.-E., Goudarzi, M.A., Nankali, H., Chéry,
728 J., Le Dortz, K., Uri, F., 2008. Monitoring of the large slow Kahrod landslide in Alborz
729 mountain range (Iran) by GPS and SAR interferometry. Engineering Geology 100, 131–141.
730 https://doi.org/10.1016/j.enggeo.2008.02.013.

731 Piacentini, D., Devoto, S., Mantovani, M., Pasuto, A., Prampolini, M., Soldati, M., 2015.
732 Landslide susceptibility modeling assisted by Persistent Scatterers Interferometry (PSI): an
733 example from the northwestern coast of Malta. Natural Hazards 78, 681-697.
734 https://doi.org/10.1007/s11069-015-1740-8.

735 Prampolini, M., Foglini, F., Biolchi, S., Devoto, S., Angelini, S., Soldati, M., 2017.
736 Geomorphological mapping of terrestrial and marine areas, northern Malta and Comino
737 (Central mediterranean sea). Journal of Maps 13(2), 457–469.
738 https://doi.org/10.1080/17445647.2017.1327507.

739 Rizzo, A., Vandelli, V., Buhagiar, G., Micallef, A.S., Soldati, M., 2020. Coastal Vulnerability
740 Assessment Along the North-Eastern Sector of Gozo Island (Malta, Mediterranean Sea).
741 Water, 12, 1405. https://doi.org/10.3390/w12051405.

742 Quinn, J.D., Rosser, N.J., Murphy, W., Lawrence, J.A., 2010. Identifying the behavioural
743 characteristics of clay cliffs using intensive monitoring and geotechnical numerical modelling.
744 Geomorphology 120(3-4), 107-122. https://doi.org/10.1016/j.geomorph.2010.03.004.

745 Scaioni, M., Longoni, L., Melillo, V., Papini, M., 2014. Remote Sensing for landslide
746 investigations: an overview of recent achievements and perspectives. Remote Sensing 6(10),
747 9600-9652. https://doi.org/10.3390/rs6109600.

748 Scerri, S., 2019. Sedimentary Evolution and Resultant Geological Landscapes, in: Gauci, R.,
749 Schembri, J. (Eds.), Landscapes and Landforms of the Maltese Islands. World
750 Geomorphological Landscapes. Springer, Cham, pp. 31-47. https://doi.org/10.1007/978-3-030-
751 15456-1_14.

752 Schön, J., 2011. Physical properties of rocks: A workbook (Vol. 8). Elsevier, Kidlington, Oxford,
753 UK.

754 Soldati, M., Barrows, T.T., Prampolini, M., Fifield, K.L., 2018. Cosmogenic exposure dating
755 constraints for coastal landslide evolution on the Island of Malta (Mediterranean Sea). Journal
756 of Coastal Conservation 22, 831-844. https://doi.org/10.1007/s11852-017-0551-3

757 Soldati, M., Devoto, S., Prampolini, M., Pasuto, A., 2019. The Spectacular Landslide-Controlled
758 Landscape of the Northwestern Coast of Malta, in: Gauci, R., Schembri, J. (Eds.), Landscapes

759 and Landforms of the Maltese Islands. World Geomorphological Landscapes. Springer, Cham,
760 pp. 167-178. https://doi.org/10.1007/978-3-030-15456-1_14.

761 Tagliavini, F., Mantovani, M., Marcato, G., Pasuto, A., Silvano, S. (2007). Validation of landslide
762 hazard assessment by means of GPS monitoring technique – A case study in the Dolomites.
763 Natural Hazards and Earth System Sciences 7(1), 185-193. https://doi.org/10.5194/nhess-7-
764 185-2007

765 Tomás, R., Abellán, A., Cano, M., Riquelme, A., Tanza-Abril, A.J., Baeza-Brotons, F., Saval,
766 J.M., Jaboyedoff, M., 2018. A multidisciplinary approach for the investigation of a rock
767 spreading on an urban slope. Landslides 15, 199-217. https://doi.org/10.1007/s10346-017-
768 0865-0.

769 Toth, C., Jóźków, G., 2016. Remote sensing platforms and sensors: A survey. ISPRS J.
770 Photogramm. Remote Sensing 115, 22-36. https://doi.org/10.1016/j.isprsjprs.2015.10.004.

771 Visser, J. P. de, 1991. Clay mineral stratigraphy of Miocene to Recent marine sediments in the
772 Central Mediterranean. Geologica Ultraiectina 75, 243

773 Wang, GQ., 2012. Kinematics of the Cerca del Cielo, Puerto Rico landslide derived from GPS
774 observations. Landslides 9, 117–130. https://doi.org/10.1007/s10346-011-0277-5.